JOURNAL OF APPLIED PHYSICS **117**, 125704 (2015)

Difference in charge transport properties of Ni-Nb thin films with native and artificial oxide

A. S. Trifonov,[1,2,a)] A. V. Lubenchenko,[3] V. I. Polkin,[4] A. B. Pavolotsky,[5] S. V. Ketov,[6] and D. V. Louzguine-Luzgin[6]

[1]*Skobeltsyn Institute of Nuclear Physics, Lomonosov Moscow State University, 1(2), Leninskie Gory, GSP-1, Moscow 119991, Russia*
[2]*Physics Faculty, Lomonosov Moscow State University, Moscow 119991, Russia*
[3]*Department of General Physics and Nuclear Fusion, National Research University "Moscow Power Engineering Institute," Moscow 111250, Russia*
[4]*National University of Science and Technology "MISiS," Moscow 119049, Russia*
[5]*Chalmers University of Technology, Göteborg 41296, Sweden*
[6]*WPI Advanced Institute for Materials Research, Tohoku University, Sendai 980-8577, Japan*

(Received 15 January 2015; accepted 11 March 2015; published online 23 March 2015)

Here, we report on the properties of native and artificial oxide amorphous thin film on a surface of an amorphous Ni-Nb sample. Careful measurements of local current-voltage characteristics of the system Ni-Nb / NiNb oxide/Pt, were carried out in contact mode of an atomic force microscope. Native oxide showed n-type conductivity, while in the artificial one exhibited p-type one. The shape of current-voltage characteristic curves is unique in both cases and no analogical behavior is found in the literature. X-ray photoelectron spectroscopy (XPS) measurements were used to detect chemical composition of the oxide films and the oxidation state of the alloy components. Detailed analysis of the XPS data revealed that the structure of natural Ni-Nb oxide film consists of Ni-NbO_x top layer and nickel enriched bottom layer which provides n-type conductivity. In contrast, in the artificial oxide film Nb is oxidized completely to Nb_2O_5, Ni atoms migrate into bulk Ni-Nb matrix. Electron depletion layer is formed at the Ni-Nb/Nb_2O_5 interface providing p-type conductivity. © *2015 AIP Publishing LLC*. [http://dx.doi.org/10.1063/1.4915935]

I. INTRODUCTION

Metallic glasses[1] and bulk metallic glasses[2,3] are a subject of significant research interest for material scientists. For example, Ni-based alloys have high glass-forming ability and millimeter-size metallic glassy rods were produced using binary Ni-Nb system alloys.[4] Ni-based metallic glasses have a high thermal stability[5,6] and good corrosion resistance.[7] In addition to a relatively large supercooled liquid region[8] and high thermal stability of these Ni-based glassy alloys, they also showed good welding ability.[9,10] A Ni-based glassy alloy also showed a very good plastic formability on heating the supercooled liquid region. Nearly full density $Ni_{52.5}Nb_{10}Zr_{15}Ti_{15}Pt_{7.5}$ bulk metallic glassy sample was produced from the powdered particles by spark plasma sintering.[11]

Glassy Ni-Nb thin films have been produced and their wear resistance,[12] as well as the effect of surface oxidation on their wear behavior,[13] optical and magnetic properties,[14] were studied. In addition, surface atomic structure of Ni-Nb bulk metallic glassy samples and their *in-situ* crystallization process were studied by scanning tunneling microscopy/ spectroscopy.[15,16]

Oxidation may induce surface crystallization of the glassy matrix.[17,18] Fine-grained microstructure consisting of ZrO_2 and Cu particles was found at the surface of $Zr_{70}Cu_{30}$ ribbons stored for a few years at room temperature[19] owing to surface oxidation. Most of Zr-based glassy alloys oxidize forming crystalline ZrO_2 particles on heating.[17] However, an amorphous phase for the oxide overgrowth on its metal substrate can be thermodynamically stable up to a certain critical thickness.[20]

On the other hand, an amorphous oxide film was formed on the surface of Ni-Nb film (native and after artificial oxidation)[14] and improved its tribological characteristics.[13] As was demonstrated,[21] Ni-Nb oxide films show non-linear current-voltage characteristics (CVCs). After annealing at 573 K for 1.8 ks, the oxide film retained its amorphous structure while at longer annealing at this temperature, nanoparticles of FCC Ni started to precipitate from the glassy Ni-Nb matrix as it gets depleted in Nb owing to its preferential oxidation forming Nb_2O_5.[14] As pure Nb_2O_5 is a dielectric material with a large bandgap and its suboxide forms can be semiconductors, it is of technological and academic importance to study the surface electrical properties of this material at metallic glass/oxide/Pt cantilever interface.

II. EXPERIMENTAL PROCEDURE

An ingot of the $Ni_{62}Nb_{38}$ alloy (alloy composition is given in nominal atomic percentages) was prepared by arc-melting the mixtures of Ni and Nb of 99.9 mass% purity in argon atmosphere. From this ingot, a target for magnetron sputtering was prepared by mechanical cutting. Thin films were deposited on Cu substrate by a magnetron sputtering technique. Deposition speed was 50 nm/min, while the

[a)]Author to whom correspondence should be addressed. Electronic mail: trifonov.artem@phys.msu.ru.

 © 2015 AIP Publishing LLC

resulted film thickness was about 100 nm. The samples were observed by scanning electron microscopy and the chemical composition of the sputtered films determined by the energy-dispersive X-ray analysis was found to be $Ni_{57}Nb_{43}$, which is slightly different from the nominal one owing to different sputtering rates of Ni and Nb. A part of the samples was later oxidized *in-situ* in the sputtering chamber at 573 K using dry air.

The phase composition of the samples was examined by X-ray diffractometry (XRD) using Rigaku Smart lab 9MTP apparatus with monochromatic CuKα. X-ray photoelectron spectroscopy (XPS) was carried out using an apparatus equipped with Scienta MX650 X-ray source of 0.2 kW power having the AlKα (1486.7 eV) radiation. The samples were moved to the XPS apparatus right after preparation or oxidation with short exposure to open air of a few hours. Each XPS analysis session was preceded by the recording of the Au $4f_{7/2}$ peak (Binding energy (BE) = 84.00 eV) for the energy calibration purpose. The sample was placed every time perpendicular to the electron energy analyzer axis. A XPS spectrum was also obtained from pure Nb sample for comparison.

Local current-voltage characteristics of Ni-Nb amorphous films containing native and artificial oxide were measured using scanning probe microscope AIST-NT SPM (model SmartSPM-1000) at ambient conditions. Contact mode of atomic force microscopy technique was used for taking topography profiles and series of local CVC's. Pt coated conductive cantilevers (Microscience, model N14/Pt) with a spring constant ranged from 6 to 10 N/m and the cantilever tip radius <40 nm were used. The spring constant was measured for each cantilever using a technique based on measuring the change in resonant frequency of the fundamental mode of vibration.[22] For each atomic force microscope (AFM) session, a new cantilever was used.

CVCs were recorded with the voltage sweeping rate of 1 ms/point, while digital feedback has been kept constant AFM cantilever load during all measurements. For statistical reproducibility, several hundred CVCs were recorded in tens regions at different cantilever load values. Almost all CVCs were reproducible. About 10% of "unusual" CVC, were recorded, probably, in the regions with some contamination absorbed on the film surface from the air.

III. RESULTS AND DISCUSSIONS

The structure of the prepared films was studied by X-ray diffraction and found to be glassy. Figure 1 shows a broad diffraction peak from 35° to 53° of 2θ typical for metallic glasses. The three sharp peaks belong to FCC Cu from the substrate. The samples annealed at 573 K for 1.8 ks and less retained its amorphous structure while, as it was shown earlier,[14] the amorphous oxide film continued to grow.

Topography of both native and artificial oxide films represents a uniformly smooth surface with a surface roughness (Rq) of 5–10 nm. Local CVC's in the native and artificial oxide films were found to be different: for native oxide, n-type conductivity observed starting from voltages −4.5 to −5.1 V, depending on the value of the load force (Figure 2(a)). The artificial oxide film revealed p-type conductivity

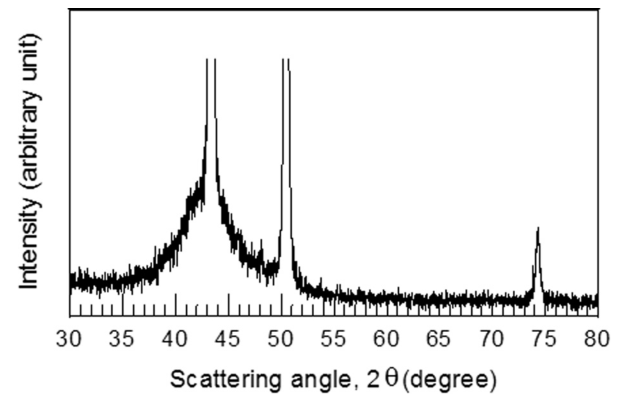

FIG. 1. XRD patterns of the as-prepared thin film. Three sharp peaks belong to FCC Cu from the substrate.

starting from +4.7 to 4.9 V (Figure 2(b)). For native oxide film, current increased in conductive region of CVC with increasing of cantilever load value (see Figure 2(a), inset) probably due to increasing of the film deformation at increasing load force. As checked by the profile measurement before and after loading the deformation of the film was elastic and non-destructive. The film "scratching" effect occurring at much higher load forces[13] was not detected in both

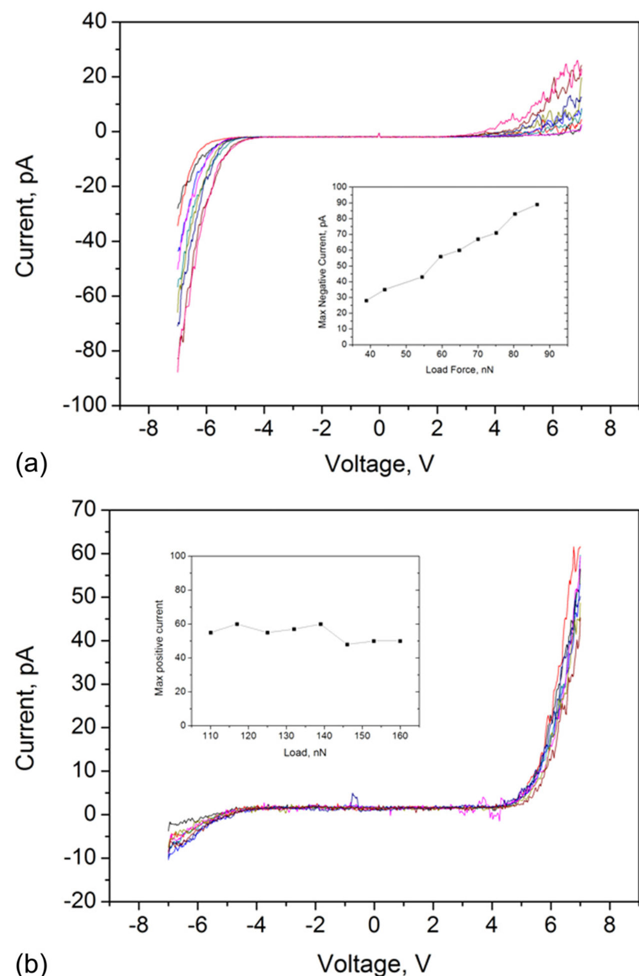

FIG. 2. A family of CVCs recorded for different cantilever loads for native (a) and artificial (b) Ni-Nb oxide films. Load ranges were from 39 to 87 nN for (a) and from 110 to 160 nN for (b). Insets show dependence of maximum current in conductive CVC region on applied cantilever load.

TABLE I. Standard XPS data results. The content of each element is given in at. %. Carbon is absorbed at the surface in terms of organic compounds.

		Ni-Nb glass	
Element	*Nb* (%)	Native oxide (%)	Artificial oxide (%)
C	41	25	25
O	48	50	61
Nb	11	13	14
Ni	…	12	…

oxides. It is worth mentioning that there was no influence of the load force on current detected for the artificial oxide film for loads up to 160 nN (see Figure 2(b), inset). Different load ranges were used for native and artificial oxides to match the measured electrical current ranges. As can be seen, the shapes of CVCs remained unchanged for the whole loads range.

One can suggest that the observed difference between the local CVCs recorded on native Ni-Nb oxide layer and that on the artificially grown oxide should be associated with the difference in the surface composition of the native and artificially grown Ni-Nb oxide layers and the oxidation state of the constituent elements. Thus, we applied XPS analysis to study the surface composition and oxidation state of the Ni-Nb oxide layers. The results of XPS analysis are presented in Table I while the spectra are shown in Figure 3.

The Nb 3d line was chosen for the Ni-Nb glass oxidation study. Here, a "line" is indicative of a series of the characteristic peaks. This line may consist of the metallic Nb doublet and the doublets corresponding to different oxidation states of Nb. As the oxidation state of Nb can be in the range from 1 to 5, it can be in total up to 12 single peaks constructing the Nb 3d. The interpretation of the recorded spectra followed the following approach. The spin-orbit doublets line shapes are described by the following relation:

$$LS_2(E) = \frac{1}{1+\alpha} \cdot \left(LS_1(E) + \alpha LS_1(E - \Delta E_{SO})\right), \quad (1)$$

where E—the photoelectron kinetic energy, $LS_1(E)$—the single line shape, α—the ratio between line intensities of spin-orbit splitting of photoelectron level ($\alpha = 1/2$ for p-orbital shell and $\alpha = 2/3$ for d-orbital shell), and ΔE_{SO}—the spin-orbit coupling energy.

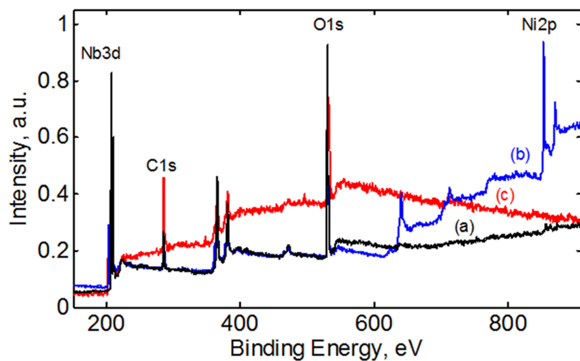

FIG. 3. XPS survey spectra: (a) Target: Nb; (b) target: Ni-Nb film on Cu (native oxide); (c) target: Ni-Nb film on Cu oxidized (artificial oxide).

The complex line shape follows the formula:

$$LS(E) = I_0 LS_2(E) + \sum_{j=1}^{N} I_j LS_2(E - \Delta E_{CS} j), \quad (2)$$

where ΔE_{CS}—the chemical shift energy, N—the highest oxidation state, and I_j—the doublet line intensity.

Following this approach, the number of varied parameters can be kept minimal: I_j and $LS_1(E)$, which are the equal for all peaks; both ΔE_{SO} и ΔE_{CS} could be taken from (Ref. 23).

For extracting the Ni-Nb surface oxide thickness, we consider the original Ni-Nb sample to be uniform and semi-infinite. We also assume that the oxidation state decreases towards the sample depth,[24] as the oxidation process proceeds only on the surface side. Following that the uniform layers can be selected where the oxidation state is constant. The number of such layers above the metallic Ni-Nb substrate will be equal to the highest oxidation state. We will number these layers so that its number corresponds to the oxidation state j of the oxide in the given layer. This way, $j = 0$ corresponds to the metallic substrate. The approach for extracting of the oxide layers thicknesses follows the earlier works.[24–26] For bi-layer sample (oxide layer with oxidation state N and thickness d over the semi-infinite metallic substrate), the thickness d can be expressed as[26]

$$d = \lambda_N \cos\theta \ln\left(\frac{n_0 \lambda_0}{n_N \lambda_N} \frac{I_N}{I_0} + 1\right), \quad (3)$$

where λ—inelastic mean free path (IMFP) of the electrons, θ—the angle of incident X-ray towards the perpendicular to the sample surface, n—concentration of the sample atoms, and I—peak intensity.

Following the same approach, the layers thicknesses in the multilayered sample can be expressed as

$$d_j = \lambda_j \cos\theta \ln\left(\frac{I_j/(n_j\lambda_j)}{\sum_{k=1}^{j-1} I_k/(n_k\lambda_k)} + 1\right). \quad (4)$$

In the relations (3) and (4), inelastic mean free paths, λj, were calculated following the TPP2M formula.[27]

The calculation results following the formulas (1)–(4) for the lines Nb 3d and Ni $2p_{3/2}$ are presented in Figure 4 showing the experimental data as points, the calculation results as solid lines and the doublet lines for different oxidation states as dashed lines. Background due to photoelectrons multiple inelastic scattering was subtracted following the Shirley method.[28] The Levenberg-Marquardt[29] algorithm was employed for line parameters extraction. The probing information depth calculated by the formula (3) for the bi-layer model ($I_5/I_0 = 100/1$) is 15 nm.

Gaussian function provides the best fit for the single line peak of the elastically scattered photoelectrons. For Nb 3d line (Figure 4(a)) obtained from the Nb sample, the following parameters were calculated:

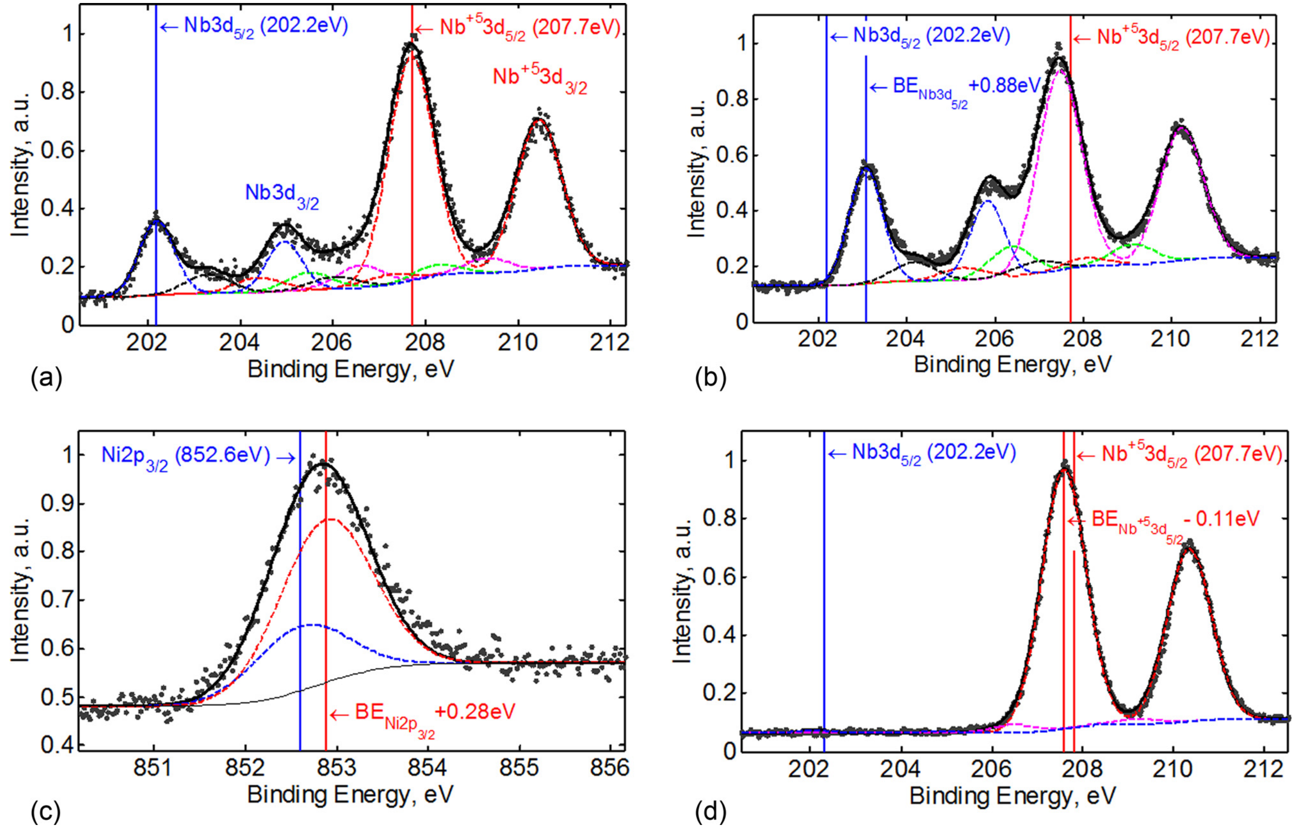

FIG. 4. XPS spectra: (a) Target: Nb; line: Nb 3d. (b) Target: Ni-Nb film on Cu (native oxide); line: Nb 3d. (c) Target: Ni-Nb film on Cu (Native oxide); line: Ni $2p_{3/2}$. (d) Target: Ni-Nb film on Cu oxidized (artificial oxide); line: Nb3d. Dotted line: experimental data; solid line: calculation by formula (2); dashed line: separate calculated peaks.

(1) Gaussian standard deviation, FWHM, equal to 0.98 eV.
(2) Binding energy for Nb $3d_{5/2}$ $BE(Nb3d_{5/2}) = 202.2$ eV.
(3) Spin-orbit coupling energy $\Delta E_{SO} = 2.75$ eV.
(4) Chemical shift energy $\Delta E_{CS} = 1.1$ eV.

The extracted Nb 3d line parameters are consistent with those reported in Ref. 23. Further on, those parameters were kept fixed. For the Ni $2p_{3/2}$ (Figure 4(c)), line parameters (FWHM = 1.02 eV, $BE(Ni\ 2p_{3/2}) = 852.6$ eV, $\Delta E_{CS} = 0.55$ eV) were taken from Ref. 30.

From the XPS data for the sample with the native Ni-Nb oxide, it was found out that all Nb 3d line peaks were shifted in respect to the $BE(Nb\ 3d_{5/2})$ by the energy $\Delta BE_{Nb} = 0.88$ eV, while the Ni $2p_{3/2}$ peak was shifted in respect to the $BE(Ni\ 2p_{3/2})$ by the energy $\Delta BE_{Ni} = 0.28$ eV. Such a peak behavior suggests that in Ni-Nb sample surface, it is Nb, which gets oxidized first, retaining though its metallic bond with Ni. Thus, the Ni-NbO_x oxide layers form over the Ni-Nb surface. Formation of the Ni-NbO_x layer causes observed electron conductivity of the native Ni-Nb oxide surface. Figure 4(b) presents comparison of the experimental data with calculations following the model presented above. Table II summarizes the oxide layers thicknesses extracted following the formula (3).

Figure 3(d) shows calculations for the Ni $2p_{3/2}$ line. Following (3), Ni-NbO_x layer is 4.2 nm thick, which is consistent with the calculations made for the Nb 3d line (Table II).

From the XPS data for the sample with the artificial Ni-Nb oxide, it was found out that all Nb 3d line peaks were shifted in respect to the $BE(Nb\ 3d_{5/2})$ by the energy $\Delta BE_{Nb} = -0.11$ eV. Ni 2p line is almost unresolved. This result can be interpreted so that Nb from Ni-Nb got completely oxidized to the highest Nb_2O_5 oxide, while Ni migrates down to the Ni-Nb substrate. On the interface between Nb_2O_5 oxide and metallic Ni-Nb, the layer with deficit of electrons forms causing the observed negative shift of the Nb 3d line in respect to the $BE(Nb3d_{5/2})$, which can be interpreted as the surface shift of the binding energy. If this surface energy shift ΔBE_{Nb} is negative, the d-zone of Ni is not completely filled, causing p-type of conductivity. Thickness of the Nb_2O_5 oxide layer calculated by the formula (3) is 10.5 nm.

Thus, the XPS data analysis showed that for native oxide Ni-Nb Nb atoms oxidized to NbO_x states but Ni-Nb bonds still remain. In an earlier work,[14] XPS of the as-cast

TABLE II. Oxide layers thicknesses (*d*) based on the XPS results.

	Metallic Nb sample		Ni-Nb alloy thin film sample	
j	Oxide composition	*d*, nm	Oxide composition	*d*, nm
1	Nb_2O		Ni-Nb_2O	0.8
2	NbO	1.6	Ni-NbO	0.3
3	Nb_2O_3	0.4	Ni-Nb_2O_3	1.1
4	NbO_2	1.2	Ni-NbO_2	2.2
5	Nb_2O_5	3.9	…	
$\sum_j d_j$		7.8		4.2

sample was measured not immediately after preparation but after some time of exposure to open air and Nb_2O_5 highest oxide was formed. Also, at that time the sample was melt spun ribbon rather than a thin film. Energy shifts on the XPS spectra of Nb 3d peaks (+0.88 eV) and Ni 2p peak (+0.28 eV) can be explained by presence of the metallic bond. In the other words, the topmost layer is Nb oxide leaving the Ni-enriched layer underneath. Such a structure demonstrates electron conductivity. In contrast, in the artificial Ni-Nb oxide layer, Nb is completely oxidized up to its highest oxide Nb_2O_5 and Ni forced to migrate down to the Ni-Nb substrate. The interface between surface Nb_2O_5 oxide and Ni-enriched Ni-Nb substrate gets deficit of electrons. This is reflected by the negative, −0.11 eV, shift of $Nb3d_{5/2}$ in respect to the binding energy. Such surface energy shift means that the d-zone of metallic Ni is less than half-filled, causing hole-type of conductivity.

Schematically, the system can be regarded as consisting of two Schottky barriers (Pt/NiO_x and NiO_x/NiNb metallic matrix), separated by the NiNb oxide tunnel barrier. The lack of conduction at voltages less than 4 V with both polarities is connected with the inability of current flow through the tunnel barrier. With the increase of the applied voltage the tunneling barrier is suppressed, allowing the charge carriers (electrons in the case of natural oxide and holes in the case of artificial oxide) to flow through the studied system.

IV. CONCLUSIONS

In conclusion, the effect of turning conductivity nature from n-type to p-type of the amorphous oxide thin film on Ni-Nb metallic glass depending on the surface oxidation state is discovered. The shape of CVC is quite unique and asymmetrical in relation with Y axis as mirror plane in both cases. It partly resembles that of a diode starting conducting at about minus or plus 5 V, respectively, with nearly total absence of conductivity at lower values and no forward/backward operating region up to about 5 V. The unique shape of CVC together with possibility of changing conductivity type by artificial oxidation indicates that this material is a promising candidate for application in a new generation of modern electronic devices.

ACKNOWLEDGMENTS

This work was supported by the Ministry of Education and Science of the Russian Federation in the framework of Increase Competitiveness Program of NUST "MISiS" (No. K2-2014-013), by the World Premier International Research Center Initiative (WPI), MEXT, Japan including WPI-AIMR Fusion Research grant "Thin native oxides on the surface of metallic glasses: an interface research" and by Russian Foundation for Basic Research, No. 14-07-00828-a.

[1]A. L. Greer, Science **267**, 1947 (1995).
[2]A. Inoue, Acta Mater **48**, 279 (2000).
[3]W. L. Johnson, MRS Bull. **24**, 42 (1999).
[4]Z. Zhu, H. Zhang, D. Pan, W. Sun, and Z. Hu, Adv. Eng. Mater. **8**, 953 (2006).
[5]D. V. Louzguine and A. Inoue, J. Non-Cryst. Sol. **337**, 161 (2004).
[6]D. V. Louzguine-Luzgin, D. B. Miracle, and A. Inoue, Adv. Eng. Mater. **10**, 1008 (2008).
[7]X. Wang, I. Yoshii, A. Inoue, Y. H. Kim, and I. B. Kim, Mater. Trans. JIM **40**, 1130 (1999).
[8]J. Y. Lee, D. H. Bae, J. K. Lee, and D. H. Kim, J. Mater. Res. **19**, 2221 (2004).
[9]D. V. Louzguine-Luzgin, G. Q. Xie, T. Tsumura, K. Nakata, Y. Murakami, H. Kimura, and A. Inoue, Ceramic Trans. **198**, 3 (2007).
[10]D. V. Louzguine-Luzgin, G. Q. Xie, T. Tsumura, H. Fukuda, K. Nakata, H. M. Kimura, and A. Inoue, Mater. Sci. Eng., B **148**, 88 (2008).
[11]G. Xie, D. V. Louzguine-Luzgin, H. Kimura, and A. Inoue, Appl. Phys. Lett. **90**, 241902 (2007).
[12]A. Caron, C. L. Qin, L. Gu, S. Gonzalez, A. Shluger, H.-J. Fecht, D. V. Louzguine-Luzgin, and A. Inoue, Nanotechnology **22**, 095704 (2011).
[13]A. Caron, P. Sharma, A. Shluger, H.-J. Fecht, D. V. Louzguine-Luzgin, and A. Inoue, J. Appl. Phys. **109**, 083515 (2011).
[14]D. V. Louzguine-Luzgin, T. Hitosugi, N. Chen, S. V. Ketov, A. Shluger, V. Yu. Zadorozhnyy, A. Caron, S. Gonzales, C. L. Qin, and A. Inoue, Thin Solid Films **531**, 471 (2013).
[15]A. I. Oreshkin, V. N. Mantsevich, S. V. Savinov, S. I. Oreshkin, V. I. Panov, N. S. Maslova, and D. V. Louzguine-Luzgin, Appl. Phys. Lett. **101**(18), 181601 (2012).
[16]A. I. Oreshkin, V. N. Mantsevich, S. V. Savinov, S. I. Oreshkin, V. I. Panov, A. R. Yavari, D. B. Miracle, and D. V. Louzguine-Luzgin, Acta Mater. **61**(14), 5216 (2013).
[17]U. Koster and L. Jastrow, Mater. Sci. Ang. A **449**, 57 (2007).
[18]Y. Wu, G. M. Song, T. Nagase, and Y. Umakoshi, J. Non-Cryst. Solids **357**, 1136 (2011).
[19]U. Koster and U. Schunemann, in *Rapidly Solidified Alloys*, edited by H. H. Liebermann (Marcel Dekker Inc., New York, 1993), p. 303.
[20]F. Reichel, L. P. H. Jeurgens, and E. J. Mittemeijer, Acta Mater. **56**, 659 (2008).
[21]V. V. Bryksin, A. V. Goltsev, S. D. Khanin, A. V. Novotelnova, and A. N. Vasilev, Phys. Status Solidi B **161**, 777 (1990).
[22]C. P. Green, H. Lioe, J. P. Cleveland, R. Proksch, P. Mulvaney, and J. E. Sader, Rev. Sci. Instrum. **75**(6), 1988 (2004).
[23]NIST X-ray photoelectron spectroscopy database—Measurement Services Division of the National Institute of Standards and Technology (NIST) Technology Services, 2008.
[24]M. Grundner and J. Halbritter, J. Appl. Phys. **51**(1), 397 (1980).
[25]T. A. Carlson, Surf. Interface Anal. **4**(4), 125 (1982).
[26]B. R. Strohmeier, Surf. Interface Anal. **15**(1), 51 (1990).
[27]S. Tanuma, C. J. Powell, and D. R. Penn, Surf. Interface Anal. **21**(3), 165 (1994).
[28]D. A. Shirley, Phys. Rev. B **5**(12), 4709 (1972).
[29]J. J. Moré, *Numerical Analysis* (Springer, Berlin Heidelberg, 1978), pp. 105–116.
[30]M. C. Biesinger, B. P. Payne, A. P. Grosvenor, L. W. Lau, A. R. Gerson, and R. S. C. Smart, Appl. Surf. Sci. **257**(7), 2717 (2011).